Progress In Electromagnetics Research, Vol. 162, 109–121, 2018

An UWB Antenna Array for Flexible IoT Wireless Systems

Haider Raad*

Abstract—In this paper a flexible compact antenna array operating in the 3.213 GHz which covers the standard UltraWide Band (UWB) frequency range is presented. The design is aimed at integration within Multiple Input Multiple Output (MIMO) based flexible electronics for Internet of Things (IoT) applications. The proposed antenna is printed on a single side of a 50.8 µm Kapton Polyimide substrate and consists of two half-elliptical shaped radiating elements fed by two Coplanar Waveguide (CPW) structures. The simulated and measured results show that the proposed antenna array achieves a broad impedance bandwidth with reasonable isolation performance ($S_{12} < -23$ dB) across the operating bandwidth. Furthermore, the proposed antenna exhibits a low susceptibility to performance degradation caused by the effect of bending. The system's isolation performance along with its flexible and thin profile suggests that the proposed antenna is suitable for integration within flexible Internet of Things (IoT) wireless systems.

1. INTRODUCTION

The growing market of the Internet of Things (IoT) calls for various types of electronic components and communication technologies for a wide spectrum of applications including smart cities and vehicles, home automation, telemedicine, and industrial applications. Obviously, the successful functionality of these applications is dependent on a reliable wireless component.

Ultra-Wide Band (UWB) systems are continuing to attract attention due to their promising advantages of low-power consumption, low cost, and high data rates. UWB is utilized in Wireless Personal Area Networks (WPAN), computer peripherals, mobile computers, imaging devices and several other applications [1]. On the other hand, UWB Multiple Input Multiple Output (MIMO) systems have been proven to further increase the channel capacity as compared to conventional band-limited MIMO systems [2]. To minimize the performance deteriorating effects of multipath fading in indoor UWB wireless communication systems diversity antenna arrays have been shown to be a practical solution, given that the radiating elements of such arrays are maintained highly uncorrelated [3].

More recently we have witnessed escalated research activities focused on the development of flexible electronics in response to the market demands which reports a growing interest in lightweight, portable, and wearable devices [4–8]. The success of flexible electronics was greatly enabled by innovations in layered semiconductors and novel fabrication techniques [9–16]. Consequently, integrating flexible UWB and MIMO antennas with such devices is ultimately needed for advanced wireless connectivity. Implementation of diversity antenna schemes for IoT applications that are subject to bending and flexing, or have curved surfaces is a challenging task due to performance degradation caused by possible structural deformation. Furthermore, the close proximity of the radiating elements in applications with limited space constraints leads to an increased mutual coupling which compromises the system's efficiency [3].

Received 8 June 2018, Accepted 29 July 2018, Scheduled 31 July 2018
* Corresponding author: Haider Raad (raadh@xavier.edu).
The author is with the Department of Physics, Xavier University, Cincinnati, USA.

Several antenna designs concerning UWB MIMO applications have been reported in the literature. These designs are mostly focused on maximizing the isolation and impedance bandwidths of the radiating elements [17–20]. In [17], an UWB monopole antenna array operating in the 2.3–7.7 GHz region has been proposed where two bent slits have been utilized to reduce the mutual coupling; $S_{12} > -18$ from 2.4 to 6.55 GHz is achieved. In [18], a printed compact UWB diversity antenna has been proposed for portable devices. The design covers only the lower UWB region (3.1–5 GHz). While in [19], a flexible UWB polarization diversity antenna with a band-notch function is proposed. Although the design demonstrates compactness and flexibility, the isolation characteristics severely deteriorate ($S_{12} > -15$) when conformed on curved surfaces.

In this paper, we present a compact half-elliptical shaped UWB monopole antenna array aimed for flexible, wearable, and conformal applications. The antenna is printed on a 50.8 µm Kapton Polyimide substrate which is known for its flexibility, robustness, low dielectric loss, and high thermal endurance. The antenna is fed by a linearly tapered Co-Planar Waveguide (CPW) to further improve the impedance matching. Furthermore, both the radiating element and ground plane are printed on the same side of the substrate which promotes lower fabrication cost and complexity in addition to roll to roll production. The proposed design exhibits reasonable isolation between the radiating elements ($S_{12} < -23$ dB) and expresses a very low susceptibility to correlation and impedance mismatch caused by the bending or conforming the antenna array. A photo of the proposed design is depicted in Fig. 1.

Figure 1. A photo of the proposed Kapton Polyimide based UltraWide Band flexible antenna array.

In Section 2, we present the antenna design aspects and fabrication process. In Section 3, we discuss the performance of the proposed antenna array in terms of isolation, radiation characteristics and flexibility. Finally, conclusions are given in Section 4.

2. ANTENNA DESIGN, CONFIGURATION, AND FABRICATION

The design of the proposed antenna array has been carried out using the full-wave electromagnetic simulation tool CST Microwave Studio which utilizes the Finite Integration Technique (FIT) time domain solver [20].

To comply with flexible technologies, integrated components are required to demonstrate high conformability and mechanical robustness simultaneously. Hence, Polyimide Kapton substrate was chosen due to its good balance of physical, chemical, and electrical properties. It has a relatively low loss tangent over a broad frequency range. Moreover, Kapton Polyimide films are available with very low thicknesses (50.8 µm) and exhibit excellent mechanical characteristics, a tensile strength of 165 MPa at 73°F, a dielectric strength of 3500–7000 volts/mil, and a temperature tolerance rating of −65 to 150°C [21].

As reported in recent literature, the radiation mechanism of planar UWB monopoles can be explained by the overlapping of closely spaced resonances. The unit radiating element of the proposed antenna array is based on a half-elliptical shaped radiating element which is a modification of a design reported previously by the author of this paper in [22]. By tuning the major axis of the radiator, the resonant frequency of the dominant mode can be constrained to cover the standard UWB region.

The radiating elements are oriented opposite to each other in a horizontal fashion to provide pattern diversity, and fed by two tapered CPWs. The linear tapering is proven to provide a smooth impedance transition which leads to a reduction in the return loss compared to a straight CPW feed. The reader is referred to [22] for further details and parametric study on the feed line tapering. The geometry and dimensions of the final array design are depicted in Fig. 2 and Table 1, respectively.

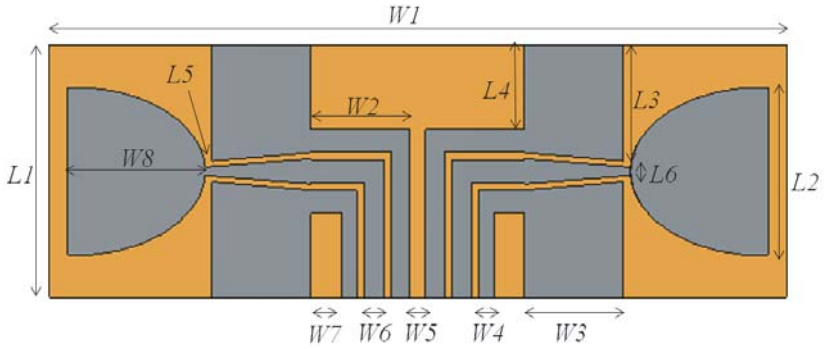

Figure 2. Geometry and dimensions of the proposed UWB printed antenna array (the grey coloured area represents the metallization of ground planes, feeding structures, and the radiating elements).

Table 1. Dimensions of the proposed UWB antenna array in millimetre.

L1	33	**W2**	15.2
L2	22	**W3**	15.2
L3	15.2	**W4**	2.5
L4	14	**W5**	2.5
L5	1.2	**W6**	3.3
L6	1.1	**W7**	5.8
W1	100	**W8**	16.5

The radiating elements along with the CPW feeding network were printed on a 50.8 µm flexible Kapton Polyimide substrate with a dielectric constant of 3.4 and a loss tangent of 0.002. A conductive solution based on sliver nanoparticles is inserted in a specialized cartridge then deposited over the Kapton substrate by a Dimatix DMP Fujifilm 2831 inkjet material printer [23]. This process is then followed by a thermal annealing at 100 C for 9 hours by an LPKF Protoflow laboratory oven. It is worth noting that two layers of ink were deposited on the substrate to achieve a consistent and continuous pattern.

3. RESULTS AND DISCUSSIONS

3.1. Scattering Parameters

Adjacently positioned antennas of distances less than a quarter wavelength could trigger high mutual coupling. This coupling can be reduced by separating the antennas at the mobile terminal. The right orientation of the antennas can disturb the phase of the surface currents and the polarization of the radiating fields. Decoupling Networks, parasitic elements, and metamaterials can be inserted between the array's elements but may affect the size, fabrication complexity, weight, and flexibility of the system. In this paper, a reasonable isolation is achieved by placing the radiating elements of the array in a back-to-back fashion with a small separation distance. This orientation gives rise to less fields interaction and yields to a change in the phases of the intersected surface currents which reduces the mutual coupling as opposed to placing the antennas adjacent to each other in a vertical fashion.

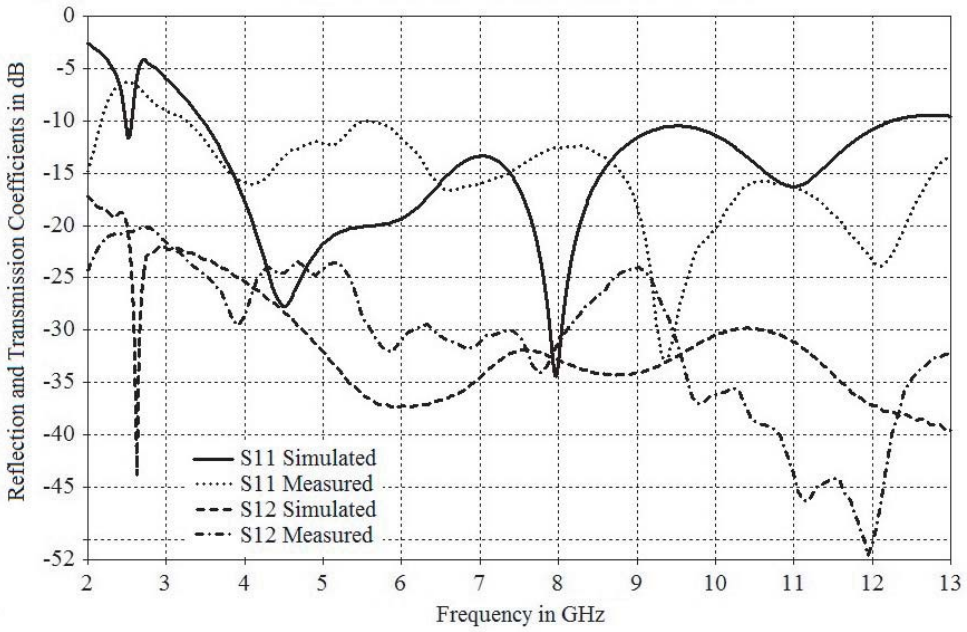

Figure 3. Simulated and measured reflection and transmission coefficients for the printed UWB antenna array.

The antenna's scattering parameters S_{11}, S_{22}, S_{21}, S_{12} were obtained using an Agilent PNA-X series N5242A Vector Network Analyzer (VNA) and compared with the simulated results from CST Microwave Studio As can be seen from the reflection coefficient graphs in Fig. 3, the measured S_{11} exhibits a -10 dB impedance bandwidth of more than 10 GHz. It extends from 3.2 GHz and goes beyond the experimental stop frequency of the VNA (13 GHz). One can also observe a resonance shifting trend that takes place beyond the 6 GHz region. However, this shift does not affect the performance of the proposed antenna since it is below the -10 dB impedance line standard. On the other hand, the simulated transmission coefficient S_{12} maintains an isolation of below -20 dB for the entire targeted frequency range In fact the isolation strengthens beyond 4.8 GHz and stays at or below -30 dB. The measured S_{12} exhibits an isolation of -23 or better for the targeted frequency range. The isolation improves further in the 5.7–8.1 GHz and beyond 9.5 GHz. The simulated and measured transmission coefficients are in fairly reasonable agreement for most parts of the bandwidth. It should also be noted that the rest of the scattering parameters (S_{22} and S_{21}) were not included in the graph below since they are redundant due to element symmetry ($S_{11} = S_{22}$, $S_{12} = S_{21}$).

3.2. Diversity Performance

Using MIMO technology in wireless data communication offers another degree of freedom and tremendously improves the data throughput. Such systems take advantage of having various propagation paths through different channels utilizing multiple antennas. At the receiving end(s), these multiple mixed signals can be treated separately. The more uncorrelated the received signals are, the higher the performance and efficiency of the MIMO systems are.

An essential figure of merit to quantify correlation effects in MIMO antenna systems is the envelope correlation coefficient which takes into account the radiation pattern characteristics, polarization, transmission coefficients and the relative phases between the radiating elements. This in turn helps with understanding the design aspects and efficiency of such systems.

In a given multipath environment, the correlation among the array's radiating elements can be deduced from the far-field information [24], mutual impedances [25], or the scattering parameters [26]. The envelope correlation can be manifested either from the far-field information which is more accurate, or from the scattering parameters. In this paper, we have used both the scattering parameters method

and the far-field method to calculate the envelope correlation using the following formulas respectively:

$$\rho = \frac{\left|S_{11}^{*}S_{12}+S_{21}^{*}S_{22}\right|^{2}}{\left(1-\left(\left|S_{11}\right|^{2}+\left|S_{21}\right|^{2}\right)\right)\left(1-\left(\left|S_{22}\right|^{2}+\left|S_{12}\right|^{2}\right)\right)} \tag{1}$$

$$\rho = \frac{\iint\limits_{4\pi} \bar{G}_1 \bar{G}_2^{*} d\Omega}{\sqrt{\iint\limits_{4\pi} \bar{G}_1 \bar{G}_1^{*} d\Omega \iint\limits_{4\pi} \bar{G}_2 \bar{G}_2^{*} d\Omega}} \tag{2}$$

Another metric used in the analysis of MIMO system which is related to the envelop correlation coefficient is the diversity gain which can be calculated from the formula below:

$$Div.\ Gain = 10 \cdot \sqrt{1-\left|\rho\right|^{2}} \tag{3}$$

where ρ is the correlation coefficient.

Figures 4 and 5 show the computed correlation coefficient and diversity gain in the 2–13 GHz range for the proposed UWB antenna array. These metrics were computed using Equations (1) and (3) which are based on the scattering parameters information. It is obvious that the array exhibits a good correlation performance in the standard UWB range (3.1–10.6 GHz) where the correlation is below 0.01. The correlation fluctuates between 0.14 and 0.01 for 2–3.1 GHz region.

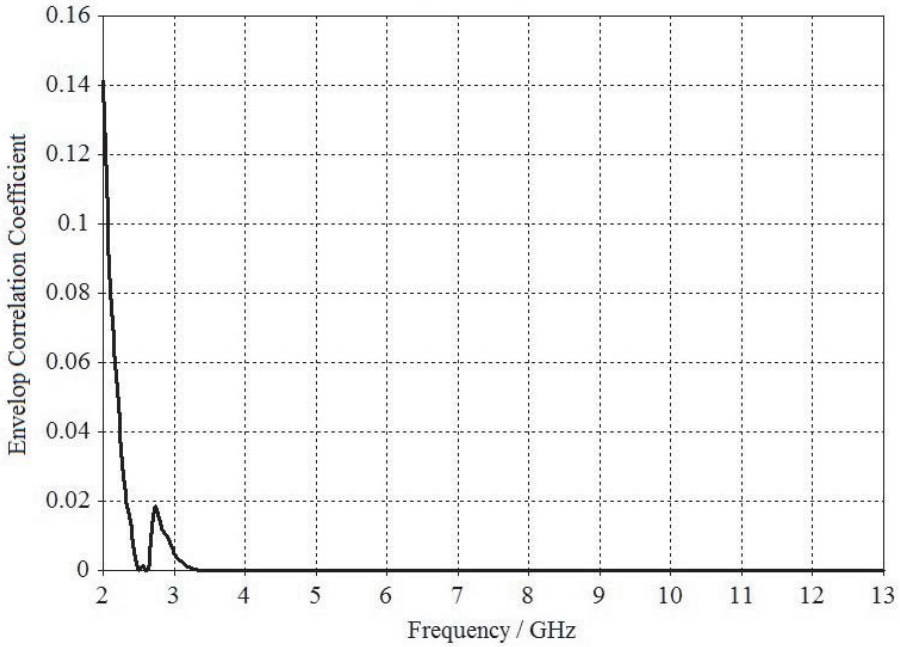

Figure 4. Calculated correlation coefficient (based on S-parameters) for the proposed UWB printed antenna array.

Figures 6 and 7 show the computed correlation coefficient and diversity gain in the 2–13 GHz range for the proposed UWB antenna array using the far-field information. It is obvious that the array exhibits a good correlation performance in the standard UWB range (3.1–10.6 GHz) where the correlation is below 0.001. The correlation fluctuates between 0.14 and 0.01 for 2–3.1 GHz region.

Envelop correlation coefficient and diversity gain are important metrics that gives a general perspective on the coupling performance. However, for practical considerations multiplexing efficiency is typically carried out by research and development facilities. Fig. 8 depicts the MIMO multiplexing efficiency for the proposed UWB array.

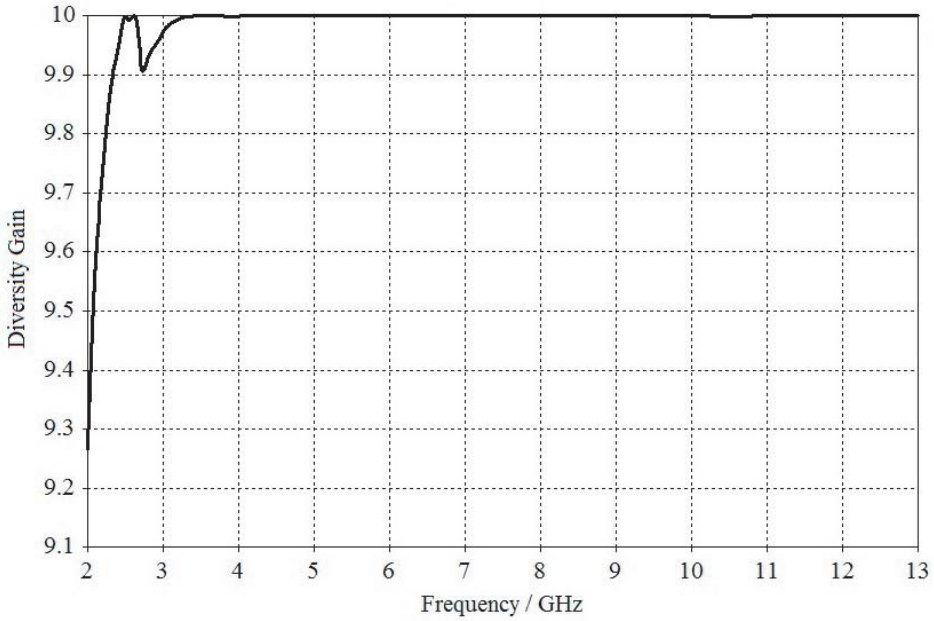

Figure 5. Calculated diversity gain (based on S-parameters) for the proposed UWB printed antenna array.

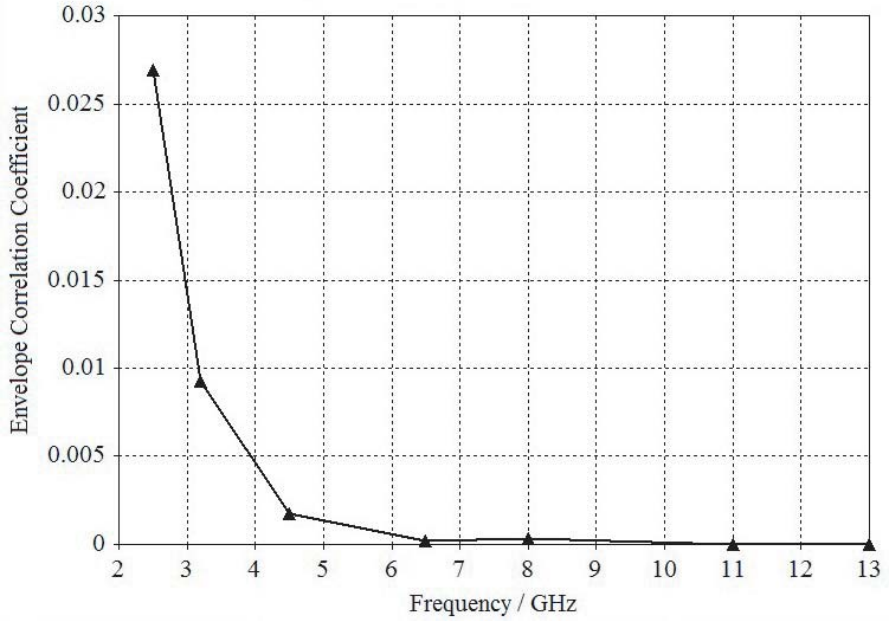

Figure 6. Calculated correlation coefficient (based on far-field data) for the proposed UWB printed antenna array.

3.3. Radiation Patterns

The E-plane (YZ cut) and H-plane (XZ cut) simulated far-field radiation patterns for four resonances across the operational bandwidth are depicted in Fig. 9. It can be seen that the radiation power is omnidirectional at 2.5 GHz, and fairly maintains such directionality at 4.5 GHz and 8 GHz. However, the radiation pattern loses omni-directionality at higher frequencies as noticed at 11 GHz.

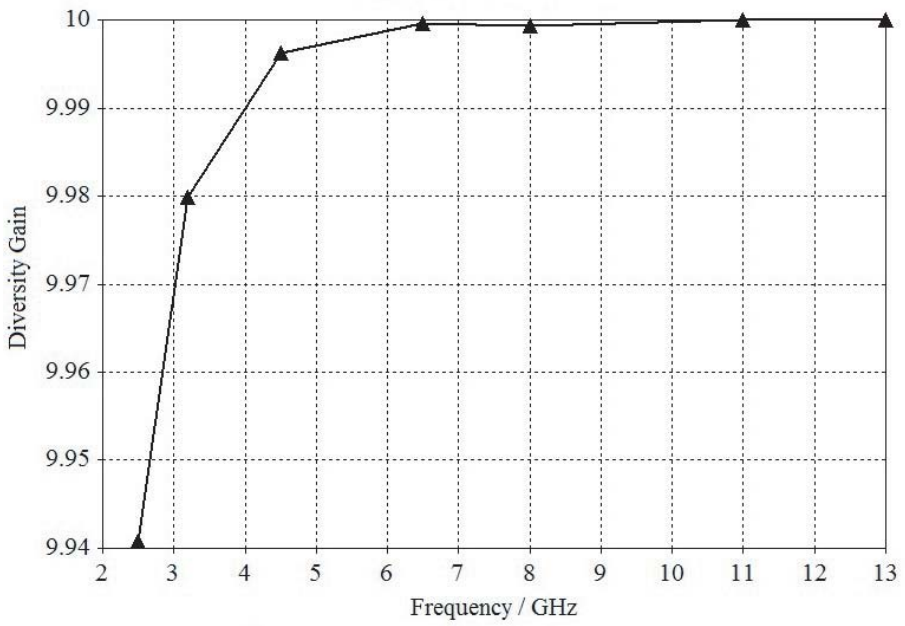

Figure 7. Calculated diversity gain (based on far-field data) for the proposed UWB printed antenna array.

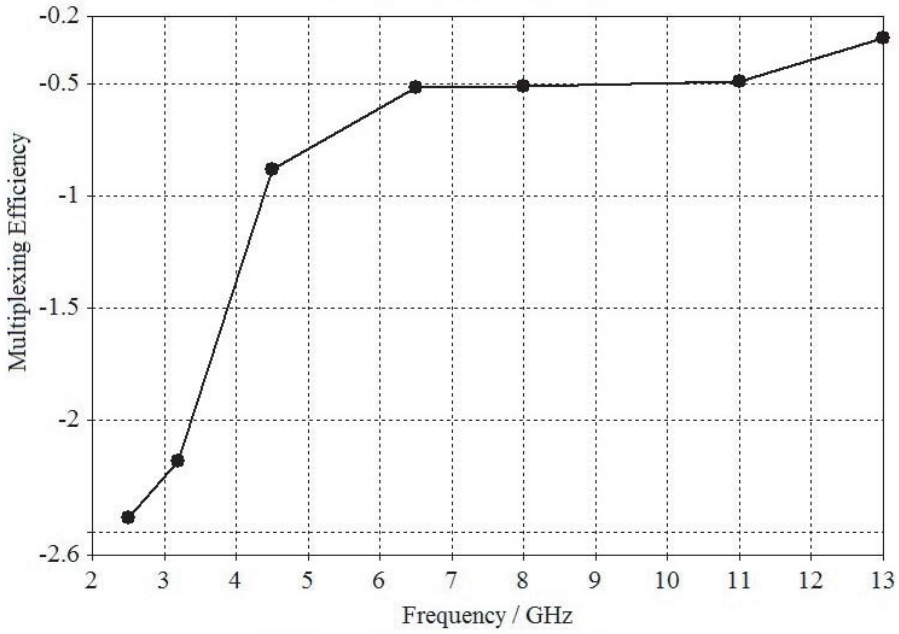

Figure 8. Calculated MIMO multiplexing efficiency (based on far-field data) for the proposed UWB printed antenna array.

3.4. Antenna Gain and Radiation Efficiency

Figure 10 depicts the peak gain values at the above-mentioned frequencies in addition to 3.1 GHz, 6.5 GHz, and 13 GHz. One can observe a higher gain value at 2.5 GHz than 3.1 GHz due to the better return loss performance at 2.5 GHz as can be seen from Fig. 3. Otherwise the gain shows an increase up to the 8 GHz region, followed by a slight decline between 8–11 GHz, then another increase between

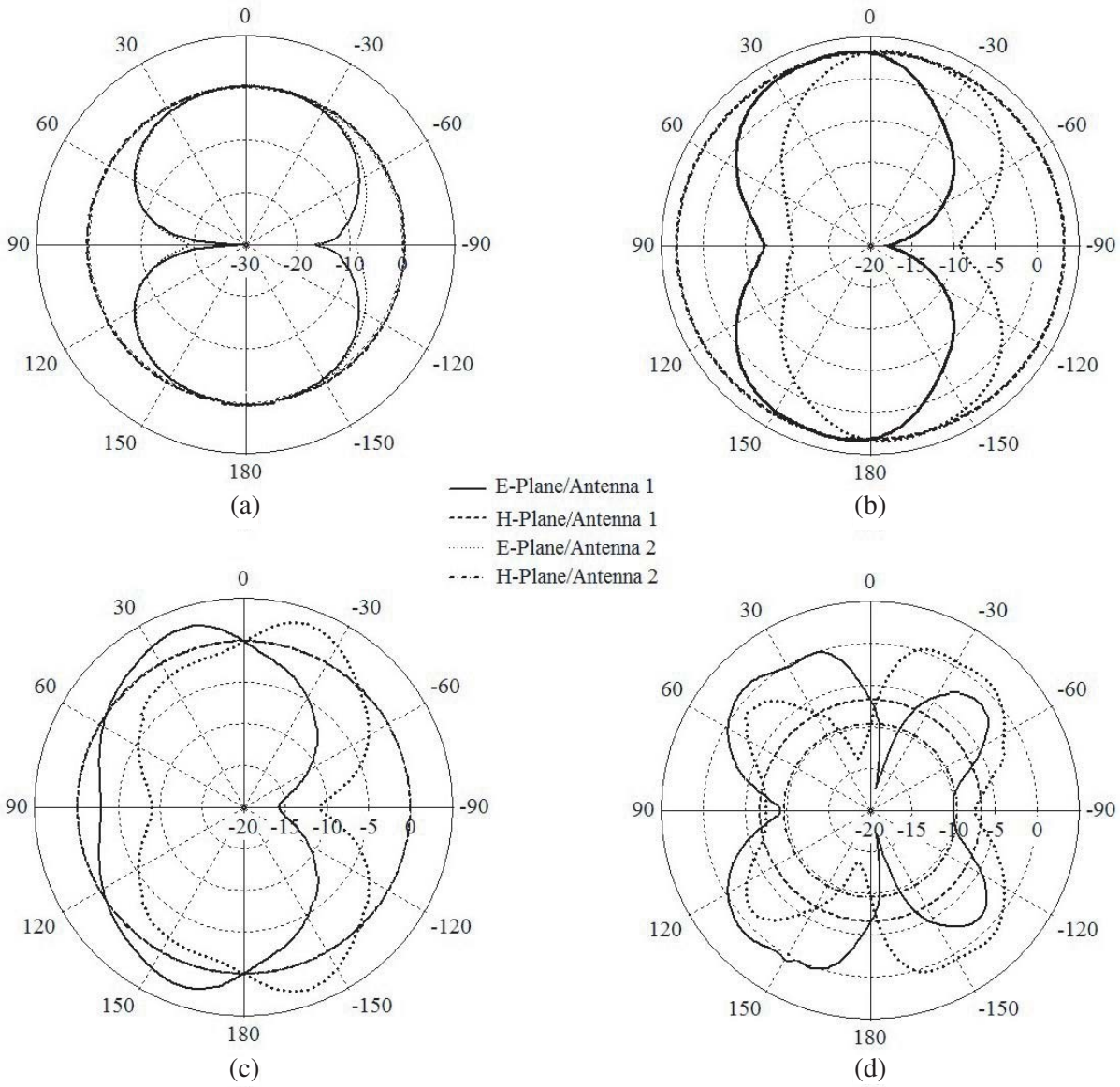

Figure 9. E-plane (YZ) and H-plane (XZ) radiation patterns for the two elements of the proposed UWB array at (a) 2.5 GHz, (b) 4.5 GHz, (c) 8 GHz, and (d) 11 GHz. Note that Antenna 1 refers to the left antenna element of the array while Antenna 2 refers to the right antenna element of the array.

11–13 GHz. It should be noted that IEEE method is used to calculate the gains at the targeted frequencies. According to IEEE Standard, the realized gain differs from the IEEE gain in that it takes into consideration the losses incurred due to the polarization mismatch and input impedance in addition to the dissipative losses (i.e., conductive and dielectric losses). Therefore, the realized gain will always be less than the intrinsic gain which considers the dissipative losses only Fig. 11 depicts the radiation efficiency over frequency which agrees with the above-mentioned gain behavior.

3.5. Flexibility Study

Since such antennas are expected to be bent, rolled, or conformed when embedded within a flexible device, some tests are needed to ensure a successful and practical operation. Scattering parameters are required to be evaluated under different degrees of bending since they are prone to change/deterioration

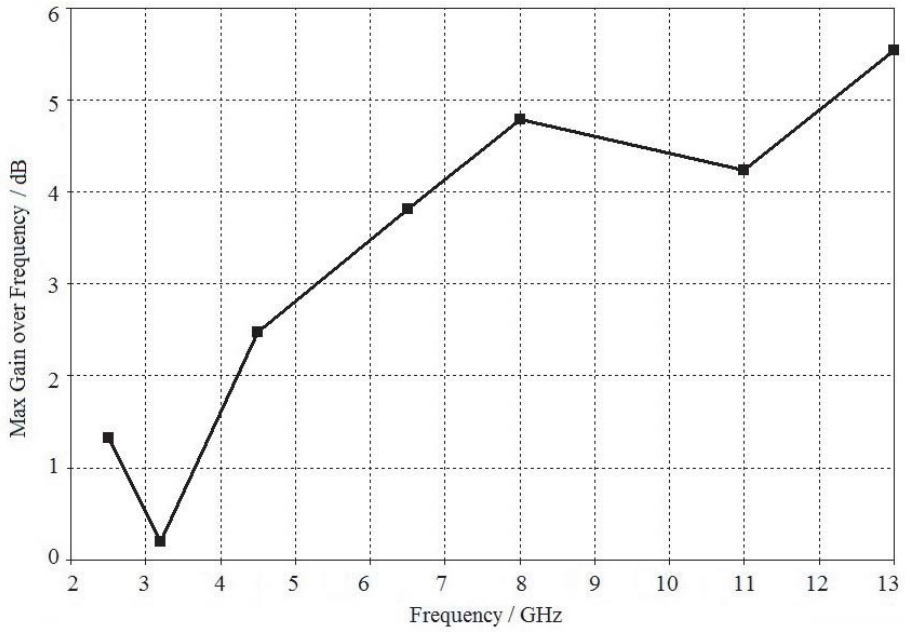

Figure 10. Maximum gain across various frequencies of the operational bandwidth of the proposed UWB antenna array.

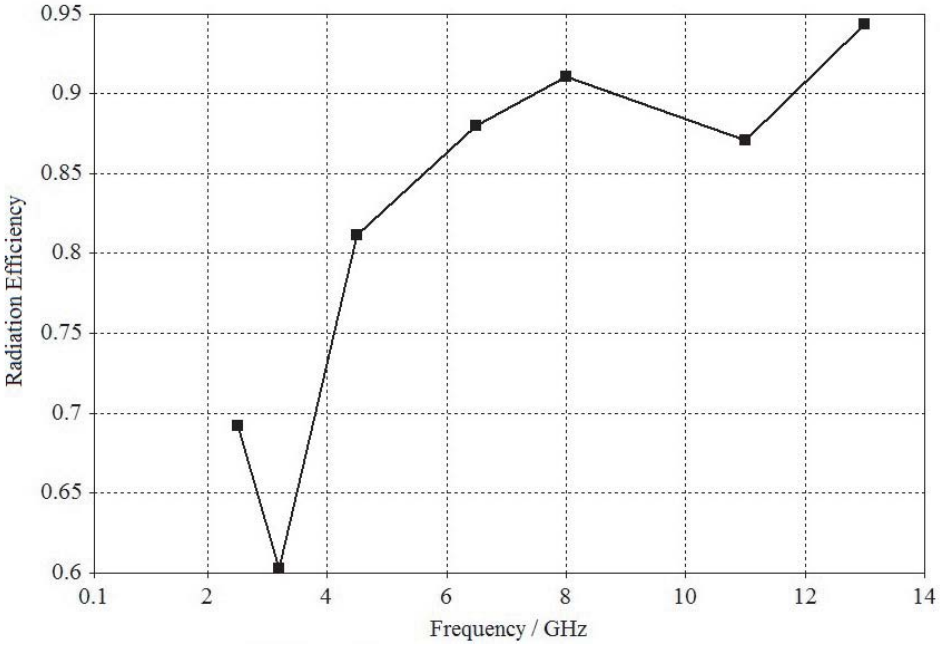

Figure 11. Radiation efficiency across various frequencies of the operational bandwidth of the proposed UWB antenna array.

due to impedance mismatch and an increased correlation between the array elements. Moreover, robustness testing of the antenna is required to verify its mechanical durability. This is performed by applying repeated bending, folding, and twisting to the antenna and check for any cracks and pattern discontinuities in the radiating element or the feeding structure via visual and/or microscopic examination if needed. Fig. 12 shows the flexibility test setup used in this paper.

To evaluate the performance of the antenna under different extents of bending, the array was conformed on foam cylinders and affixed using a temporary adhesive tape. Two foam cylinders with different radii have been used to emulate two different extents of bending.

As seen from Fig. 13, a slight deterioration in the return loss occurs around 6 GHz when the antenna is bent on the foam cylinder with 40 mm which represents a mild degree of bending. On the other hand, the return loss experiences more deterioration in the 5.5 GHz when the antenna is bent on the cylinder with 30 mm radius which represents the more severe bending case. Moreover, there is also a slight resonance shift to the lower side of the range.

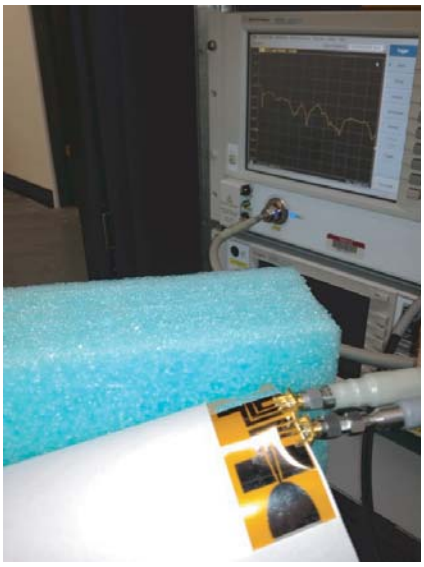

Figure 12. Flexibility test setup (the proposed antenna array is conformed over a cylindrical foam with different radii to emulate different extents of bending).

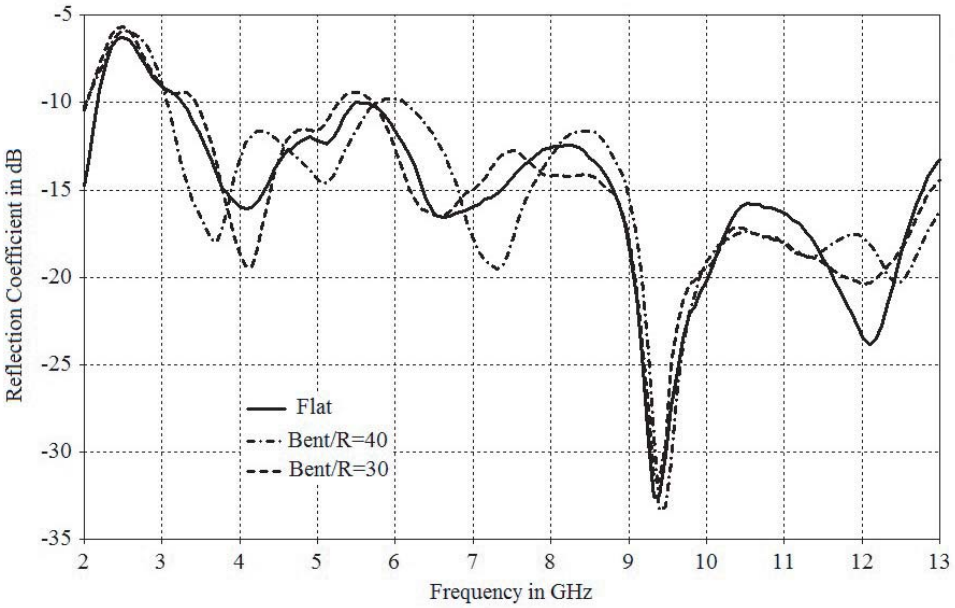

Figure 13. Measured reflection coefficients S_{11} of the proposed UWB antenna array when bent on foam cylinders with different radii ($r = 40$ mm and $r = 30$ mm) to mimic different bending extents.

On the other hand, a proportional increase in mutual coupling to the bending extent is observed as evident from Fig. 14. The deterioration is more prominent in the 3–4.8 GHz region when bent on the 40 mm cylinder, while the degradation extends even further (3.8–7.4 GHz) when the antenna is bent on the 30 mm cylinder. This is attributed to the fact that the effective separation distance between the radiating elements decreases, in addition to the radiation pattern intersection when the structure is curved which conflicts with the concept of pattern diversity.

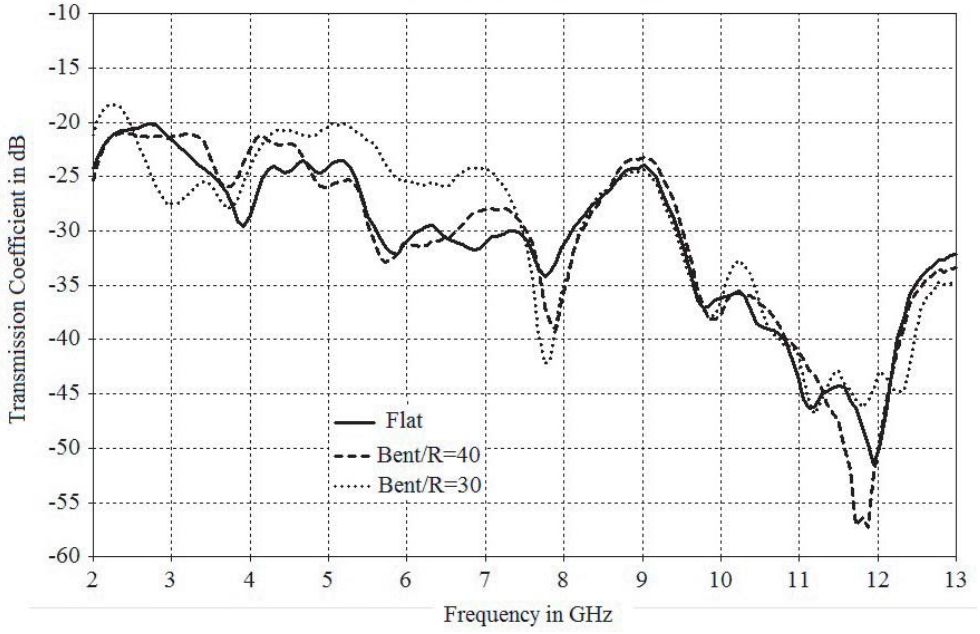

Figure 14. Measured transmission coefficients S_{12} of the proposed UWB antenna array when bent on foam cylinders with different radii ($r = 40$ mm and $r = 30$ mm) to mimic different bending extents.

Table 2. Comparison with recent UWB array designs.

Characteristics	**Proposed**	**Ref. [27]**	**Ref. [28]**	**Ref. [29]**	**Ref. [30]**
Size in mm	100×22	170×170	80×50	46×32.6	36×36
Thickness	50.8 µm	3.94 mm	1.57 mm	1.6 mm	1.6 mm
Bandwidth	> 10 GHz	1.43 GHz	≈ 3.5 GHz	> 10 GHz	≈ 8 GHz
Isolation Perf.	> 23 dB	> 25 dB	> 22.1 dB	≈ 20 dB	> 15 dB
Correlation Coefficient	≤ 0.001	≤ 0.7	Not reported	≤ 0.006	≤ 0.12
Diversity Gain	> 9.98	> 9.3	Not reported	> 9.94	Not reported
Multiplexing Efficiency	> -2.2 dB	Not reported	Not reported	Not reported	Not reported
Fabrication Complexity	Simple, single layer	Medium, two layers	Medium, two layers	Complex, Multi-layer	Medium, two layers
Flexibility	Yes	Yes	Yes	No	No

3.6. Comparative Study

The antenna array proposed in this paper is compared to four different types of UWB antenna arrays reported in the literature [27–30]. Given the applications envisioned in this paper, the comparative study is emphasized on size, thickness, flexibility, fabrication complexity, isolation performance, correlation coefficient, diversity gain, and multiplexing efficiency. Table 2 shows the above-mentioned comparison factors.

Clearly, the proposed design offers a lower profile, simpler fabrication process, and larger impedance bandwidth than the reported designs adopted in this comparison. The proposed array also offers a better isolation performance than the other designs except for [27]; however, the design reported in [27] is relatively larger in size (170 mm × 170 mm) than the proposed design (100 mm × 22 mm).

4. CONCLUSION

A flexible compact UWB MIMO/diversity antenna system is proposed in this paper. The wideband isolation is achieved by orienting the radiating elements of the array in a back-to-back fashion with a simple spatial diversity. The proposed antenna is printed on a single side of a 50.8 µm Kapton Polyimide substrate and consists of two half-elliptical shaped radiating elements with a tapered CPW feeding structure. The simulated and measured results show that the proposed antenna array achieves a broad impedance bandwidth with reasonable isolation across the operating bandwidth ($S_{12} < -23$ dB). Moreover, the proposed antenna exhibits a relatively low susceptibility to performance deterioration due to bending. The array's diversity performance, simple fabrication process, along with its flexible and thin profile suggest that it would be a reasonable candidate for integration within flexible and wearable devices in Internet of Things (IoT) applications.

REFERENCES

1. Awais, Q., H. Tariq Chattha, M. Jamil, Y. Jin, F. A. Tahir, and M. Ur Rehman, "A novel dual ultrawideband CPW-fed printed antenna for Internet of Things (IoT) applications," *Wireless Communications and Mobile Computing*, Vol. 10, 1–9, 2018.
2. Tao, J. and Q. Feng, "Compact ultrawideband MIMO antenna with half-slot structure," *IEEE Antennas and Wireless Propagation Letters*, Vol. 16, 792–795, 2017.
3. Ren, J., D. Mi, and Y. Yin, "Compact ultrawideband MIMO antenna with WLAN/UWB bands coverage," *Progress In Electromagnetics Research C*, Vol. 50, 121–129, 2014.
4. Raad, H., H. Al-Rizzo, A. Isaac, and A. Hammoodi, "A compact dual band polyimide based antenna for wearable and flexible telemedicine devices," *Progress In Electromagnetics Research C*, Vol. 63, 153–161, 2016.
5. Raad, H., A. Abbosh, H. M. Al-Rizzo, and D. G. Rucker, "Flexible and compact AMC based antenna for telemedicine applications," *IEEE Transactions on Antennas and Propagation*, Vol. 61, No. 2, 524–531, Feb. 2013.
6. Khaleel, H. R., H. Al-Rizzo, and D. Rucker, "Compact polyimide-based antennas for flexible displays," *IEEE Journal of Display Technology*, Vol. 8, No. 2, 91–97, Feb. 2012.
7. Al-Adhami, Y. and E. Erçelebi, "Plasmonic metamaterial dipole antenna array circuitry based on flexible solar cell panel for self-powered wireless systems," *Microw. Opt. Technol. Lett.*, Vol. 59, 2365–2371, 2017.
8. Al-Adhami, Y. and E. Ercelebi, "A plasmonic monopole antenna array on flexible photovoltaic panels for further use of the green energy harvesting," *Progress In Electromagnetics Research M*, Vol. 68, 143–152, 2018.
9. Politano, A., L. Viti, and M. Vitiello, "Optoelectronic devices, plasmonics, and photonics with topological insulators," *APL Materials*, Vol. 5, 035504, 2017.
10. Viti, L., A. Politano, and M. Vitiello, "Black phosphorus nanodevices at terahertz frequencies: Photodetectors and future challenges," *APL Materials*, Vol. 5, 035602, 2017.

11. Politano, A., M. S. Vitiello, L. Viti, D. W. Boukhvalov, and G. Chiarello, "The role of surface chemical reactivity in the stability of electronic nanodevices based on two-dimensional materials "beyond graphene" and topological insulators," *Materials Science (cond-mat.mtrl-sci)*; *Mesoscale and Nanoscale Physics, FlatChem 1*, 60–64, 2017.
12. Politano, A., G. Chiarello, R. Samnakay, G. Liu, B. Gurbulak, S. Duman, A. Balandin, and D. Boukhvalov, "The influence of chemical reactivity of surface defects on ambient-stable InSe-based nanodevices," *Nanoscale*, Vol. 8, 1039, 2016.
13. Weinan, Z., P. Saungeun, N. Maruthi, K. Yogeesh, M. McNicholas, R. Seth, and A. Deji, "Black phosphorus flexible thin film transistors at gigahertz frequencies," *Nano Letters*, Vol. 16, 2301, 2016.
14. Weinan, Z., N. Maruthi, S. Yogeesh, S. Yang, H. Aldave, K. Joon-Seok, S. Sushant, L. Tao, L. Nanshu, and A. Deji, "Flexible black phosphorus ambipolar transistors, circuits and AM demodulator," *Nano Letters*, Vol. 15, No. (3), 1883–1890, 2015.
15. Akinwande, D., N. Petrone, and J. Hone, "Two-dimensional flexible nanoelectronics," *Nat. Commun.*, Vol. 5, 5678, 2014.
16. Boukhvalov, D., B. Gürbulak, S. Duman, L. Wang, A. Politano, L. Caputi, G. Chiarello, and A. Cupolillo, "The advent of indium selenide: Synthesis, electronic properties, ambient stability and applications," *Nanomaterials*, Vol. 7, No. 11, 3390, 2017.
17. Wong, K., S. Su, and Y. Kuo, "A printed ultra-wideband diversity monopole antenna," *Microw. Opt. Technol. Lett.*, Vol. 38, 257–259, 2003.
18. See, T. S. P. and Z. N. Chen, "An ultrawideband diversity antenna," *IEEE Transactions on Antennas and Propagation*, Vol. 57, No. 6, 1597–1605, 2009.
19. Yoon, H. K., Y. J. Yoon, H. Kim, and C. Lee, "Flexible ultra-wideband polarisation diversity antenna with band-notch function," *IET Microwaves, Antennas and Propagation*, Vol. 5, No. 12, 1463–1470, 2011.
20. http/www.cst.com.
21. Dupont Kapton Polyimide specification sheet, www2.dupont.com/kapton.
22. Khaleel, H., H. Al-Rizzo, D. Rucker, and S. Mohan, "A compact polyimide-based UWB antenna for flexible electronics," *IEEE Antennas and Wireless Propagation Letters*, Vol. 11, 564–567, 2012.
23. http://www.fujifilmusa.com/products/industrial inkjet print heads/index.html.
24. Vaughan, R. and J. Andersen, "Antenna diversity in mobile communications," *IEEE Trans. Veh. Technol.*, Vol. 36, No. 4, 149–172, 1987.
25. Hui, H. and H. Lui, "Expression of correlation coefficient for two omindirectional antennas using conventional mutual impedances," *Electron. Lett.*, Vol. 44, No. 20, 1177–1178, 2008.
26. Blanch, S., J. Romeu, and I. Corbella, "Exact representation of antenna system diversity performance from input parameter description," *Electron. Lett.*, Vol. 39, No. 9, 705–707, 2003.
27. Castel, T., S. Lemey, P. Van Torre, C. Oestges, and H. Rogier, "Four-element ultrawideband textile cross array for dual-spatial and dual-polarization diversity," *IEEE Antennas and Wireless Propagation Letters*, Vol. 16, 481–484, 2017.
28. Ahmed, M., E. Abdallah, and H. Elhennawy, "Novel wearable eagle shape microstrip antenna array with mutual coupling reduction," *Progress In Electromagnetics Research B*, Vol. 62, 87–103, 2015.
29. Raj, K., R. Krishna, and N. Kushwaha, "Design of a compact MIMO/diversity antenna for UWB applications with modified TH-like structure," *Microwave and Optical Technology Letters*, Vol. 58, 1181–1187, 2016.
30. Zhao, H., F. Zhang, X. Zhang, and C. Wang, "A compact band-notched ultra-wideband spatial diversity antenna," *Progress In Electromagnetics Research C*, Vol. 51, 19–26, 2014.